JACS
JOURNAL OF THE AMERICAN CHEMICAL SOCIETY

ARTICLE

pubs.acs.org/JACS

Oxidation of Au by Surface OH: Nucleation and Electronic Structure of Gold on Hydroxylated MgO(001)

Matthew A. Brown, Yuichi Fujimori, Franziska Ringleb, Xiang Shao, Fernando Stavale, Niklas Nilius, Martin Sterrer,* and Hans-Joachim Freund

Department of Chemical Physics, Fritz-Haber-Institut der Max-Planck-Gesellschaft, Faradayweg 4-6, D-14195 Berlin, Germany

Supporting Information

ABSTRACT: The nucleation and electronic structure of vapor-deposited Au on hydroxylated MgO(001) surfaces has been investigated under ultrahigh vacuum conditions. Hydroxylated MgO(001) surfaces with two different hydroxyl coverages, 0.4 and 1 monolayer, respectively, were prepared by exposure to water (D_2O) at room temperature. Scanning tunneling microscopy experiments show significantly higher gold particle densities and smaller particle sizes on the hydroxylated MgO surface as compared to gold deposited on clean MgO(001). Infrared spectroscopy and X-ray photoelectron spectroscopy experiments were performed to reveal details about the initial nucleation of gold. Gold atoms are found to chemically interact with a specific type of hydroxyl groups on the MgO surface, leading to the formation of oxidized gold particles. The enhanced adhesion of Au particles, which is due to the formation of strong Au−O interfacial bonds, is responsible for the observed higher stability of small Au clusters toward thermal sintering on hydroxylated MgO surfaces. The results are compared to similar studies on Au/TiO_2(110) model systems and powder samples prepared by the deposition−precipitation route.

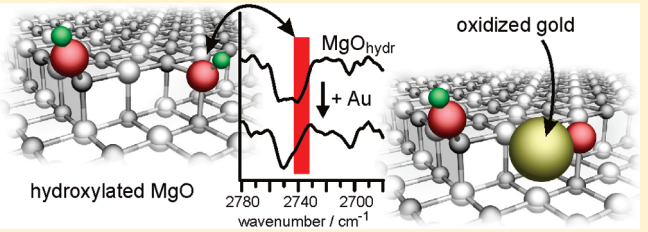

1. INTRODUCTION

Hydroxyl groups on oxide surfaces are of paramount importance to surface chemistry and interface phenomena. As reactive surface functional groups, hydroxyls determine the acid−base chemistry and catalysis of oxide materials.[1] They are directly involved in the early stages of catalyst preparation as surface ligands for anchoring metal complexes[2] and have been suggested to actively participate in many catalytic reactions over oxide-supported metal particles (e.g., in CO oxidation over oxide-supported Au particles).[3] Moreover, hydroxyl groups, among other parameters such as surface termination and surface defects,[4−6] modify the electronic and chemical interaction at metal/oxide interfaces, which opens a possibility for tuning the properties of metal/oxide heterojunctions for future nanotechnology applications.[7,8] Clearly, understanding the macroscopic properties related to hydroxyls on oxide surfaces requires knowledge of their properties and interactions with atoms and molecules at a fundamental level. In this study, we reveal details of the chemical interaction of gold atoms with hydroxyl groups on a MgO(001) model surface. The results allow us to conclude about the initial nucleation site as well as about the relationship of electronic structure and spectroscopic properties of gold species on the hydroxylated MgO(001) surface.

Supported gold nanoparticles are known to be catalytically active for a number of reactions including oxidation of CO and hydrocarbons, synthesis of H_2O_2, etc.[9] In CO oxidation, the catalytic performance of oxide-supported gold catalysts is found to be influenced by several factors including Au particle size,[10−12] oxidation state of gold,[13−15] and nature of the oxide support.[16] Apart from those, the potential role of water and hydroxyls in catalysis over supported Au nanoparticles has been highlighted recently. High activity in CO oxidation has been found for colloidal Au particles deposited on $Mg(OH)_2$ and is attributed to the enhanced supply of active oxygen on the hydroxylated support.[17] As a coreactant, small doses of water were shown to increase the catalytic activity in CO oxidation, which is partly attributed to activation of oxygen and to the transformation of tightly bound carbonate, which acts as a poison, into bicarbonate species that are able to release CO_2 at moderate temperature.[18] In situ high-pressure studies addressing the influence of co-fed water in CO oxidation over model Au/TiO_2(110) surfaces have, however, not been conclusive in this respect.[19,20] In addition, hydroxyl species on the oxide support represent strong anchoring sites for the solution complexes during preparation of gold catalysts by the deposition−precipitation method,[21] and this interaction has been suggested to determine the final structure—in particular, high dispersion and small particle sizes—of supported Au nanoparticles.[22,23] This conclusion is substantiated by the observation of nanometer and subnanometer Au particles after deposition−precipitation of Au on $Mg(OH)_2$ and $Fe(OH)_3$ supports.[24,25]

Fundamental ultrahigh vacuum (UHV) surface science studies combined with calculations have provided a basic insight

Received: May 25, 2011
Published: June 02, 2011

dx.doi.org/10.1021/ja204798z | J. Am. Chem. Soc. 2011, 133, 10668–10676

into energetics and morphological properties of metal deposits on well-characterized, single-crystalline oxide surfaces.[4−7] Most of the experimental studies have been carried out with pristine oxide surfaces, devoid of any functional surface groups. However, in any realistic environment, the oxide termination is subject to changes according to the thermodynamic equilibrium imposed by the environment, and in almost all cases an oxide will be covered by a certain amount of strongly bound hydroxyl groups after exposure to air and at moderate temperature. Therefore, under the pristine conditions of an UHV experiment, a materials gap is known to exist, which makes extrapolating the fundamental insight gained in an UHV environment to that of powder materials in a realistic environment a difficult proposition. In order to bridge this materials gap, several groups reported on the selective modification of single-crystalline oxide surfaces with hydroxyl groups by exposure to water and investigated the properties of subsequently deposited metals. The metals studied—Al, Ti, Rh, Co, and Cu—were shown to become oxidized by the interaction with surface OH groups.[8,26−31] According to the different interaction strengths found for Al, Co, and Cu, a correlation of the reactivity of the metal toward OH and its oxygen affinity was proposed.[29] Recently, the adsorption energy of atomic oxygen was shown to be a good descriptor for the activation energy of water splitting on a given metallic surface.[32] According to this finding, Au surfaces are by far the least active among the transition metals investigated, in line with the expected inertness of gold. On the other hand, the interaction strength toward oxygen is considerably enhanced for low-coordinated gold sites present on nanoparticles as opposed to extended gold faces,[33] implying that a certain reactivity may be expected toward oxidation by OH for the smallest Au particles. In fact, Wang and Hammer,[34] modeling adsorption of Au_7 clusters on TiO_2(110) surfaces with terminal OH groups, found strong binding of these clusters to the surface and positive charging of the interfacial Au atoms. On the other hand, in recent UHV experiments that addressed the effect of water on the nucleation properties of Au on TiO_2(110), bridging hydroxyl groups formed by water dissociation on oxygen vacancies were consistently shown to enhance sintering of Au on TiO_2 as compared to a reduced surface, implying a weaker metal−support interaction on the hydrated TiO_2(110) surface.[35−37] The different results for Au on TiO_2(110) suggest that nucleation and diffusion properties strongly depend on the chemical nature of the various OH groups present on the surface.

In this article, we provide a detailed picture of the nucleation and electronic structure of gold on hydroxylated MgO(001) model surfaces by analyzing the complementary experimental results obtained from scanning tunneling microscopy (STM), X-ray photoelectron spectroscopy (XPS), and infrared spectroscopy. In particular, we are able to identify a site-selective interaction of Au with hydroxyl groups on this surface, which results in oxidized gold particles. Furthermore, the comparison of stretching frequencies of adsorbed CO and corresponding Au 4f binding energies of the supported Au particles as a function of annealing temperature allows for a rigorous correlation of infrared and XPS characteristics, two properties that are most frequently applied to determine the active state of supported gold in heterogeneous catalysis research.

2. EXPERIMENTAL SECTION

The experiments were preformed in a UHV chamber equipped with a hemispherical electron energy analyzer (Specs Phoibos 150) together with a twin-anode X-ray source (Specs XR50) for X-ray photoelectron spectroscopy (XPS), and a low-energy electron diffraction (LEED) system. A small UHV-compatible high-pressure cell connected to the main UHV chamber was used for hydroxylation of the MgO(001) substrate as well as for infrared experiments in (grazing) reflection absorption geometry (IRAS).

The Ag(001) sample was mounted by Ta wires to Mo rods on the manipulator and could be heated to 673 K or cooled with liquid nitrogen to 100 K. The temperature was monitored via a chromel−alumel thermocouple (K-type) spot-welded to the back side of the crystal. The Ag(001) single crystal used as substrate for the growth of MgO(001) thin films was cleaned by repeated sputter−anneal cycles. Stoichiometric 13 monolayer (ML) MgO(001) films were grown by reactive deposition of Mg in an oxygen ambient of 1×10^{-6} mbar of O_2 at a substrate temperature of 573 K and a deposition rate of 1 ML/min. The surface quality was verified with LEED and the stoichiometry of the film with XPS.

Gold nucleation and sintering was studied on three different MgO(001) surfaces characterized by different surface coverage, θ, of hydroxyl groups: Clean MgO(001), which contains a negligible amount of OH, and MgO(001) samples dosed for 3 min at room temperature at 1×10^{-3} mbar and 1 mbar water vapor pressures. According to our previous quantitative estimations, dosing at 1×10^{-3} mbar results in θ(OH) ∼ 0.4 ML hydroxyl coverage.[38] This sample will be referred to as MgO with low hydroxyl coverage, $MgO_{hydr(l)}$. MgO with high hydroxyl coverage of θ(OH) ∼ 1.0 ML is obtained after dosing 1 mbar water vapor and is referred to as $MgO_{hydr(h)}$. (All water dosing experiments were performed with D_2O. However, the term hydroxylation instead of deuteroxylation will be used throughout the paper.) Annealing the MgO_{hydr} films to 600 K desorbs weakly bound hydroxyl groups, which reduces the coverage to θ(OH) ∼ 0.1 ML and θ(OH) ∼ 0.3 ML for $MgO_{hydr(l)}$ and $MgO_{hydr(h)}$, respectively. Gold was deposited on the surface of clean MgO(001) and MgO_{hydr} either at 100 K or at room temperature in UHV by physical vapor deposition at a rate of 0.1 Å/min (1 ML ≈ 2.5 Å).

Photoelectron spectra were collected by use of Al Kα radiation (1486.6 eV) at an electron takeoff angle of 60°. The hemispherical energy analyzer was set to constant pass energy of 20 eV. Fitting the two components of the O 1s region in MgO_{hydr} (OH at high binding energy and O^{2-} of MgO at low binding energy) is straightforward and has been previously presented in the literature.[38] The Au 4f and Mg 2s spectral regions overlap and require additional care when fitting (see description in the Supporting Information). The magnesium and oxygen binding energies of MgO_{hydr} are subject to downward shifts compared to MgO(001) because of band bending caused by hydroxylation.[38] For 13 ML MgO/Ag(001), the shift is as large as −0.7 eV for hydroxylation at 1×10^{-3} mbar D_2O and −0.4 eV at 1 mbar D_2O. Since the binding energy of Au deposited on MgO_{hydr} is also affected by these shifts, we used as reference the binding energies of samples that have been annealed to 573 K to remove the OH species. After this treatment, the substrate binding energies are similar for both MgO(001) and MgO_{hydr} (530.5 eV for O 1s and 88.9 eV for Mg 2s). The binding energy scale of the XP spectra obtained at lower annealing temperature (Figures 1 and 5) has been corrected according to the shift determined with respect to the reference spectrum.

IR spectra with CO as a probe molecule were collected at 100 K and at grazing incidence on a Bruker IFS66v/S spectrometer and a liquid nitrogen-cooled mercury−cadmium−telluride (MCT) detector. Each spectrum was obtained by averaging 1000 interferograms with a spectral resolution of 4 cm^{-1}. Background measurements were collected from the clean MgO and MgO_{hydr} samples before deposition of gold. CO dosages are given in Langmuir units (1 L = 1.33×10^{-6} mbar·s).

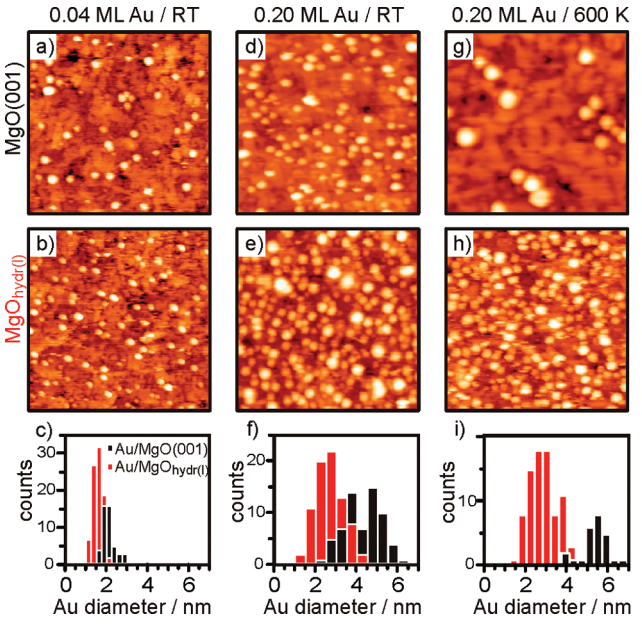

Figure 1. STM micrographs (50 nm × 50 nm) of 0.04 and 0.20 ML Au deposited at room temperature on clean (a, d) and hydroxylated (b, e) surfaces of 10 ML MgO(001)/Mo(001), and after annealing of the 0.2 ML Au samples to 600 K (g, h). The hydroxyl coverage in panels b and e is ~0.4 ML, corresponding to $MgO_{hydr(l)}$. Tunneling conditions: i_t = 0.1 nA, U_s = +5−6 V. The Au particle size distributions are presented in panels c, f, and i, respectively [black = Au/MgO(001); red = Au/MgO_{hydr}].

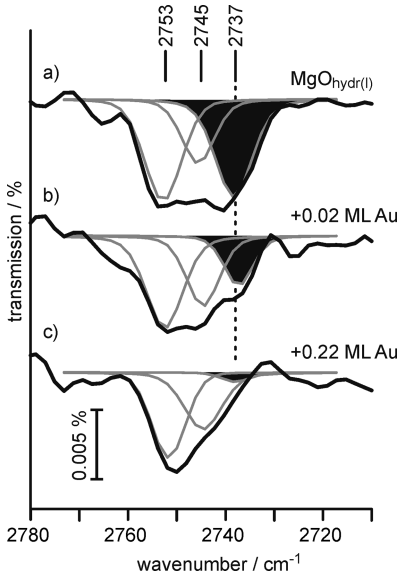

Figure 2. IR spectra taken at room temperature after (a) hydroxylation of 13 ML MgO(001)/Ag(001) at p(D_2O) = 1 × 10^{-3} mbar for 3 min [$MgO_{hydr(l)}$], (b) subsequent deposition of 0.02 ML Au, and (c) additional deposition of 0.20 ML Au.

The STM experiments were performed in a different UHV chamber. For STM measurements, MgO(001) thin films of 10 ML thickness were grown on Mo(001) as support and Au was evaporated at room temperature by procedures similar to those described above. Surface hydroxylation was achieved by water dosing through a doser at a background pressure of 1 × 10^{-5} mbar of H_2O at a distance of 1 mm to the sample, giving an effective pressure of 1 × 10^{-3} mbar of H_2O at the sample surface. All STM images shown here were acquired at room temperature in the constant current mode.

3. RESULTS

3.1. Interaction of Au with Water and Hydroxyls on MgO(001) and MgO_{hydr}. We have first analyzed the nucleation behavior of Au on hydroxylated MgO in real space. Figure 1 shows representative STM images and particle size distributions obtained after deposition of 0.04 ML Au (Figure 1a−c) and 0.20 ML Au (Figure 1d−f) on clean and hydroxylated (1 × 10^{-3} mbar of D_2O) MgO, respectively. A significant increase in gold particle density, n, on hydroxylated MgO as compared to MgO(001) is observed: 0.042 nm^{-2} on MgO_{hydr} versus 0.023 nm^{-2} on MgO(001) for 0.04 ML Au, and 0.098 nm^{-2} on MgO_{hydr} versus 0.017 nm^{-2} on MgO(001) for 0.20 ML Au. In line with the increased particle density, the Au particle diameter, d, is smaller on hydroxylated MgO. When tip convolution effects are taken into account, a mean diameter of 1.5 nm was estimated for 0.04 ML Au on hydroxylated MgO, whereas it is 2.0 nm on MgO(001) [2.5 and 4−5 nm for 0.20 ML Au on MgO_{hydr} and MgO(001), respectively]. The difference between Au on MgO(001) and MgO_{hydr} becomes even more pronounced after annealing the sample to elevated temperature. The STM micrographs shown in Figure 1g,h for 0.2 ML Au after annealing to 600 K show that large three-dimensional particles form on MgO(001) with strongly reduced particle density (0.007 nm^{-2}) compared to the unannealed state (Figure 1d, 0.017 nm^{-2}). In contrast, both particle density (0.10 nm^{-2}) and particle diameter (2.6 nm) remain almost unaffected upon annealing of the MgO_{hydr} surface. Since the thermal energy exceeds the diffusion barriers for Au atoms and small clusters on the regular MgO(001) surface under the experimental conditions applied here,[39] it is safe to assume that nucleation and growth of Au on the MgO(001) surface proceeds at particular surface sites, such as step edges or point defects. The higher Au particle density on the hydroxylated MgO surface suggests that additional nucleation centers are created by surface hydroxylation. It is not possible to extract detailed morphological information about the Au nucleation centers present on the MgO surfaces from the STM images shown in Figure 1.

Spectroscopic evidence for the nature of the additional nucleation centers on MgO_{hydr} is provided in Figure 2, which shows IRAS spectra of the OD region from the MgO surface that has been exposed to 1 × 10^{-3} mbar of D_2O, and after subsequent deposition of 0.02 and 0.22 ML Au at room temperature (RT). The spectrum of the hydroxylated MgO surface (Figure 2a) contains signal contributions at ν(OD) = 2737, 2745, and 2753 cm^{-1}. Upon deposition of 0.02 ML Au, the band at 2737 cm^{-1} is reduced in intensity (Figure 2b), and by increasing the amount of deposited Au (0.22 ML, Figure 2c), this band is almost completely depleted. None of the other hydroxyl signals is affected. Two important conclusions can be drawn from the IRAS results presented in Figure 2. First, the loss of the OD IR signal indicates that hydroxyls are consumed by interaction with gold. This result is analogous to previous findings, for example, for Rh deposited on hydroxylated alumina.[40] Second, this interaction is selective and affects only particular hydroxyl groups, primarily those that give rise to a stretching frequency of ν(OD) = 2737 cm^{-1}. The results presented above suggest that Au becomes oxidized upon selective nucleation at hydroxyls.

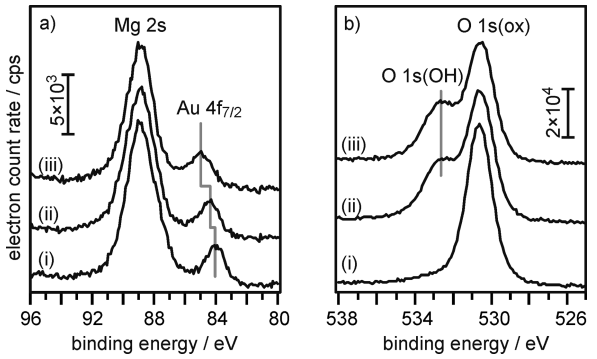

Figure 3. XPS spectra of the (a) Au 4f and (b) O 1s spectral regions for 0.04 ML Au (i) deposited at room temperature on 13 ML MgO(001)/Ag(001) and (ii) after subsequent hydroxylation at 1 mbar of D_2O. (iii) Spectra obtained after deposition of 0.04 ML Au on hydroxylated (1 mbar of D_2O) 13 ML MgO(001)/Ag(001).

To obtain more information about changes in the electronic structure of Au induced by its interaction with OH, we performed XPS and IRAS using CO as a probe.

3.2. Electronic Structure of Au on MgO(001) and MgO_{hydr}. Figure 3 displays the results of XPS measurements for 0.04 ML Au (i) deposited at room temperature on a clean MgO(001) surface, (ii) after subsequent hydroxylation of the surface, and (iii) for 0.04 ML Au deposited at RT on hydroxylated MgO(001). A binding energy of 84.0 eV for the Au $4f_{7/2}$ component in spectrum i of Figure 3a is consistent with the formation of metallic Au particles on clean MgO(001). Subsequent exposure of the surface to 1 mbar of water at RT leads to complete hydroxylation of the MgO surface, as evident from the additional O 1s component at 532.7 eV [O 1s(OH)] typical for hydroxyl groups on MgO (spectrum ii in Figure 3b).[38] After posthydroxylation treatment, the Au $4f_{7/2}$ signal is found at 84.3 eV, shifted by 0.3 eV to higher binding energy compared to the clean MgO surface (Figure 3a). Recently, it was shown that the shape of supported Au particles is subject to dynamical changes during H_2-O_2 cycling experiments, with chemisorbed oxygen at millibar exposures of O_2 being responsible for rounding of the otherwise octahedral particles.[41] Along the same lines, the binding energy shift of the Au $4f_{7/2}$ component after posthydroxylation (Figure 3a) can be attributed to a change in the chemical nature of the Au particles due to chemisorption of hydroxyl groups, which result either from direct water interaction with the small Au particles or from spillover of hydroxyl groups from the oxide support onto the Au particles.

If gold is deposited at room temperature onto the hydroxylated MgO surface, the Au $4f_{7/2}$ binding energy is shifted to even higher values as compared to the posthydroxylation experiment, and the maximum appears at ~85.0 eV (spectrum iii in Figure 3a). The electronic structure of the Au particles formed on the hydroxylated MgO surface cannot be unambiguously determined from the XPS spectrum in Figure 3, because both final and initial state effects can contribute to the observed XPS chemical shift. Initial state effects[42] refer to local electron density of the atom from which the photoelectron originates and could arise from oxidized gold species, where the gold core level binding energy is known to shift higher.[43] On the other hand, final state effects[44] are of particular concern for small metal clusters supported on insulating substrates and refer to the influence of screening of the positive charge created after electron

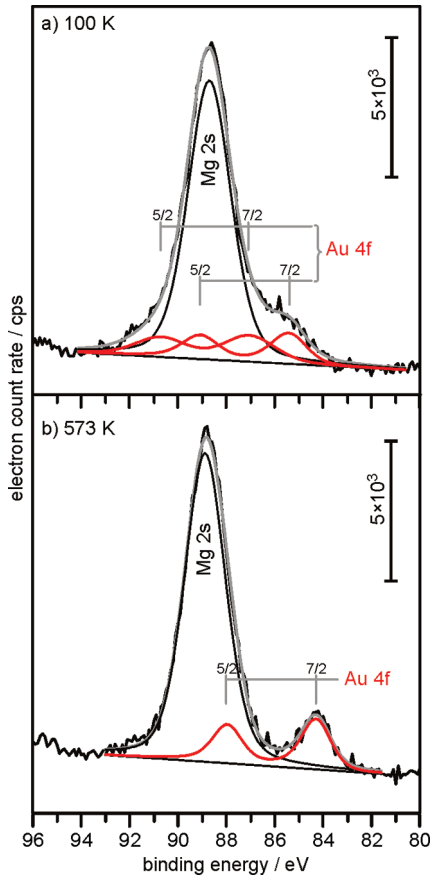

Figure 4. Experimental photoemission spectra and results of fits of the Mg 2s and Au 4f region for 0.02 ML Au (a) deposited at 100 K onto 13 ML $MgO_{hydr(l)}$ and (b) of the same sample after annealing to 573 K.

detachment, which will raise the core level binding energy.[45,46] Deconvoluting the positive shift into initial and final state contributions has proven to be an experimental challenge. Typically, the most applied method is the Auger parameter analysis;[47] however, gold's weak Auger emission renders this sort of procedure feasible only for samples with high gold loading or at synchrotron facilities. Our approach is to use the complementary results of XPS and IRAS to qualitatively separate the two.

In order to obtain more detailed insight into the electronic structure of Au on hydroxylated as compared to clean MgO surfaces, we probed the evolution of Au-specific spectroscopic features in XPS as a function of temperature. We have performed a complete temperature series between 100 and 600 K, and the spectra were fit to evaluate the temperature dependence of distinct Au oxidation states. Two examples are presented in Figure 4, which shows Au 4f XPS spectra and fits obtained for 0.02 ML Au on $MgO_{hydr(l)}$ (a) directly after deposition at 100 K and (b) after annealing to 573 K. [A description of the fitting procedure and XPS spectra and fits for 0.02 ML Au on MgO(001), $MgO_{hydr(l)}$, and $MgO_{hydr(h)}$ at various annealing temperature can be found in the Supporting Information.]

In Figure 5 we compare the binding energy of the Au $4f_{7/2}$ components as a function of annealing temperature for 0.02 ML Au on the three different MgO surfaces. On MgO(001), two components with Au $4f_{7/2}$ binding energies of 84.4 and 85.6 eV, respectively, are present after deposition of Au at 100 K (Figure 5a). The binding energy of the former component increases slightly

dx.doi.org/10.1021/ja204798z |J. Am. Chem. Soc. 2011, 133, 10668–10676

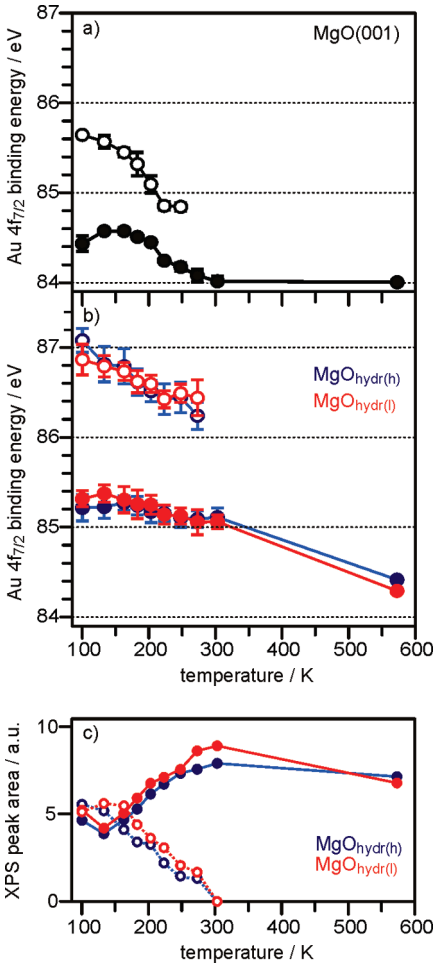

Figure 5. Au $4f_{7/2}$ binding energies as a function of annealing temperature obtained from fits of the photoemission spectra for 0.02 ML Au deposited at 100 K on (a) 13 ML MgO(001)/Ag(001) and (b) $MgO_{hydr(l)}$ (red) and $MgO_{hydr(h)}$ (blue). (c) Au 4f peak area as a function of annealing temperature for Au/$MgO_{hydr(l)}$ (red) and Au/$MgO_{hydr(h)}$ (blue). Open and solid symbols represent the high and low Au $4f_{7/2}$ binding energy components, respectively.

upon annealing to 130 K, probably due to thermally induced rearrangement of the small Au species on the MgO surface. Upon further annealing, the binding energy of both components tends downward and the two components merge into a single one at ~240 K, which at 300 K exhibits a binding energy of 84.1 eV and reaches the bulk Au value of 84.0 eV after heating to 573 K.[48]

A similar trend is visible in the annealing series for Au deposited on the hydroxylated MgO samples (Figure 5b). Compared with Au on MgO(001), however, the Au $4f_{7/2}$ binding energies are higher at all annealing temperatures. After deposition at 100 K, the low binding energy component is found at 85.3 and 85.2 eV on $MgO_{hydr(l)}$ and $MgO_{hydr(h)}$, respectively, and remains almost constant up to an annealing temperature of 300 K. Only after heating to 573 K does the binding energy shift to lower values, 84.3 eV [$MgO_{hydr(l)}$] and 84.4 eV [$MgO_{hydr(h)}$]. The second Au component at high binding energy exhibits values of 86.9 eV [$MgO_{hydr(l)}$] and 87.1 eV [$MgO_{hydr(h)}$] directly after deposition at 100 K. With increasing temperature, the binding energy of this component shifts to lower values (Figure 5b) and the peak intensity decreases steadily between 150 and 270 K (Figure 5c). At 300 K it has completely vanished on both $MgO_{hydr(l)}$ and $MgO_{hydr(h)}$ surfaces, and the spectra show only a single Au 4f component. The binding energy shifts observed for Au deposited at low temperature on MgO_{hydr} of up to +3 eV compared to bulk Au (84.0 eV) are significantly higher than the maximum contribution expected from final state effects, which is reported to be in the range +1.0 to +1.5 V.[49] Therefore, the XPS data provide strong evidence that the initial nucleation of gold on hydroxyls leads to oxidized gold species on the surface. This statement can be confirmed by complementary IRAS studies of CO adsorbed on Au particles that have been prepared under the same conditions as in the XPS experiments described above. CO IRAS is particularly suited for this purpose because the CO stretching vibration is a sensitive probe of the Au oxidation state.[50]

Figure 6 shows the IRAS spectra taken following a 1 L exposure of CO at 100 K for 0.02 ML Au on 13 ML MgO(001)/Ag(001) (black, upper spectra), $MgO_{hydr(l)}$ (red, middle spectra), and $MgO_{hydr(h)}$ (blue, lower spectra) as deposited (a) at 100 K and after annealing to (b) 300 or (c) 600 K. All spectra were collected at 100 K. The CO IRAS spectra for 0.02 ML Au on MgO(001) have been described in detail previously[48] and are presented here for comparative reasons. At 100 K on MgO(001), three distinct absorption bands at 2170, 2154, and 2121 cm^{-1} are evident. The former two signals are assigned to cationic gold species nucleated at defect sites such as anion vacancies (F^{2+}) and grain boundaries, while the band at 2121 cm^{-1} originates from CO adsorption on small metallic Au clusters or at the oxide-cluster periphery. With annealing to 300 K, a single broad absorption feature with weak intensity centered around 2110 cm^{-1} remains, which is due to CO adsorption on flat, 2 ML high Au particles. Continued annealing to 600 K results in a single sharp band centered at 2090 cm^{-1}, which is characteristic for CO on three-dimensional, metallic Au particles. In addition to the IR bands reported in Figure 6, the contribution of CO adsorbed on single Au atoms on MgO(001) at 1850 cm^{-1} is detected at 100 K (data not shown).[48] The atoms are, however, unstable toward agglomeration at higher temperature and are lost after annealing to 140 K.

On $MgO_{hydr(l)}$, two broad absorption bands are initially present at 100 K centered around 2165 and 2125 cm^{-1}, the latter exhibiting a shoulder at 2135 cm^{-1}. At 300 K the main spectral contribution is a band at 2130 cm^{-1}. By 600 K a single sharp band remains at 2090 cm^{-1} with an intensity 2 times that seen on Au/MgO(001). At 100 K on $MgO_{hydr(h)}$, two broad features at 2170 and 2130 cm^{-1} are observed. These bands are blue-shifted with respect to Au on $MgO_{hydr(l)}$ and the intensity of the band at 2170 cm^{-1} is significantly reduced. After annealing to 300 K, the spectrum is similar to that of Au on $MgO_{hydr(l)}$, with a band centered at 2130 cm^{-1} but with a smaller absorption intensity. By 600 K, a single band remains at 2088 cm^{-1} with a signal intensity between that of MgO(001) and $MgO_{hydr(l)}$. On both $MgO_{hydr(l)}$ and $MgO_{hydr(h)}$, no contribution of CO adsorbed on neutral Au atoms could be detected. The IR data presented in Figure 6c indicate that the chemical state of Au after a final anneal to 600 K is the same on all MgO surfaces investigated here and corresponds to metallic Au particles. At lower temperature, however, the CO adsorption properties on MgO_{hydr}-supported Au particles are slightly altered as compared to those on clean MgO(001) (Figure 6a,b) pointing to differences in both morphology and chemical state of Au on these surfaces.

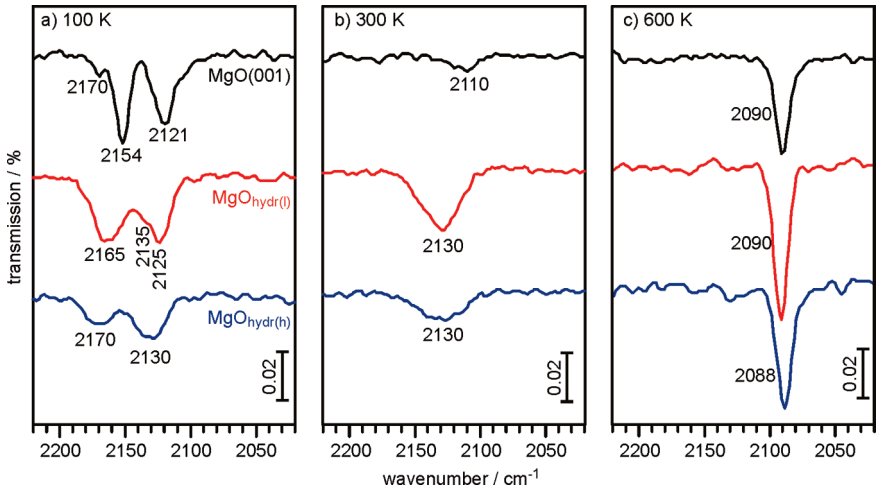

Figure 6. IR spectra of adsorbed CO on 0.02 ML Au on (upper, black) 13 ML MgO(001)/Ag(001), (middle, red) $MgO_{hydr(l)}$, and (lower, blue) $MgO_{hydr(h)}$ as a function of annealing temperature: (a) 100, (b) 300, or (c) 600 K. Spectra were all collected at 100 K following a 1 L exposure of CO.

4. DISCUSSION

Combining the STM, XPS, and IRAS results presented in the previous section provides us with the ability to draw a very detailed picture of the initial nucleation of Au atoms on the hydroxylated MgO(001) surface with regard to the nature of nucleation sites and Au chemical state. As evidenced by the IRAS results presented in Figure 2, only a particular type of hydroxyl group [with ν(OD) = 2737 cm^{-1}] is able to chemically interact with incoming gold atoms. Based on previous experimental findings for MgO powders and more recent density functional theory (DFT) calculations, frequencies in the range 2730−2760 cm^{-1} can be attributed to dicoordinated, isolated hydrogen-bond acceptor hydroxyls (at lower frequency) and single-coordinated hydrogen-bond acceptor hydroxyls (at higher frequency).[51,52] More specifically, an experimental study carried out for MgO smoke particles and thin films combined with computations identified a hydroxyl group with ν(OH) = 3710 cm^{-1} [which corresponds to ν(OD) = 2735 cm^{-1} when an isotopic factor of 1.356 is taken into account][51] as dicoordinated OH groups on step edges.[53,54] Support for this assignment comes from our own studies on the pressure-dependent hydroxylation of 12 ML MgO(001)/Ag(001) films, where a band at ν(OD) = 2737 cm^{-1} was detected at low H_2O pressure,[38] corresponding to water dissociation at highly reactive surface sites, most likely at step edges. Although some ambiguity still remains in the exact assignment of OH groups on MgO, the studies mentioned above enable conclusions about the relationship of certain surface structural elements and associated stretching frequencies of OH groups on MgO.[52−54] On the basis of this correlation, we assign the hydroxyl band at ν(OD) = 2737 cm^{-1}, and therefore the Au nucleation site on hydroxylated MgO, to dicoordinated hydroxyl groups formed by water dissociation at low-coordinated step sites.

The chemical nature of the Au species nucleated at hydroxyl groups is inferred from the combined IRAS and XPS results presented in Figures 4−6. Before going into the details of the Au/MgO_{hydr} samples, it is useful to recall the results of the temperature-dependent behavior of 0.02 ML Au deposited on clean MgO(001), which has been discussed previously.[48] Briefly, the Au $4f_{7/2}$ binding energy component at 85.6 eV and the IR absorptions at 2154 and 2170 cm^{-1} observed at 100 K have been assigned to small, cationic Au_n (n = 2, 3) clusters nucleated at defects such as anion vacancies and grain boundaries that act as electron trapping sites. The Au $4f_{7/2}$ component at 84.5 eV and the IR band at 2121 cm^{-1}, on the other hand, are attributed to small, metallic Au clusters.[48] Annealing to elevated temperature promotes diffusion and agglomeration of the small Au species, leading to larger Au particles. Hence, the binding energy of both components shifts to lower values. The shift of the lower binding energy component is attributed to the better final state screening in larger particles, whereas the shift of the higher binding energy component is due to dilution of the initial positive charge upon attachment of neutral atoms. By 240 K, only one Au $4f_{7/2}$ component at 84.2 eV remains, which shifts to 84.1 eV at 300 K and to 84.0 eV at 600 K, consistent with the formation of large, metallic Au nanoparticles.[48]

The XPS and IRAS results for Au on hydroxylated MgO surfaces show qualitatively similar trends compared to those for Au on MgO(001). However, the details reveal differences in the chemical nature of the Au species as well as their morphology over the entire temperature range investigated. We first note the high binding energy Au $4f_{7/2}$ components at 86.9 and 87.1 eV observed at 100 K on $MgO_{hydr(l)}$ and $MgO_{hydr(h)}$, respectively, which fall into the range reported for Au_2O_3 and strongly oxidized gold clusters.[43,55] The disappearance of these species after annealing to 300 K coincides with the loss of the CO band at 2165−2170 cm^{-1}, suggesting a direct relationship between these XPS and IRAS signals. The second Au $4f_{7/2}$ component is recorded at 85.2 eV on hydroxylated MgO surfaces, which is shifted by 0.7 eV to higher binding energy than the corresponding low binding energy Au $4f_{7/2}$ component on MgO(001) at this temperature. In addition, the binding energy of this component stays almost constant in the temperature range between 100 and 300 K on MgO_{hydr}, whereas on MgO(001) it decreases to 84.1 eV. Because of the rather limited mobility of Au at 100 K and the small Au coverage (0.02 ML), the initial cluster sizes at 100 K are not expected to differ significantly from one support to the other. We, therefore, exclude that final state effects contribute to the binding energy difference observed for 0.02 ML Au on MgO_{hydr} and MgO(001) and assign the Au $4f_{7/2}$ component at 85.2 eV on MgO_{hydr} also to oxidized gold. Support for this assignment is provided by the CO IRAS results

for Au on MgO_{hydr}, where signals in the area of 2130 cm^{-1}, blue-shifted with respect to CO on metallic gold particles, are observed at 100 and 300 K, respectively.

Upon annealing to 573 K, a single Au species with a binding energy of 84.4 eV remains on MgO_{hydr}, shifted by +0.4 eV relative to that of bulk Au. This temperature is high enough to facilitate complete reduction of the oxidized Au particles into the metallic state,[55] a fact that is corroborated by the IRAS results showing a similar CO stretching frequency of ~2090 cm^{-1} for the annealed Au particles on all MgO supports. The higher binding energy for Au on MgO_{hydr} as compared to MgO(001) after annealing to 573 K is, therefore, mainly ascribed to the final state effect, suggesting that the Au particles are significantly smaller on MgO_{hydr}. The latter conclusion is in agreement with our previous TPD study, which provided evidence for higher Au dispersion on MgO_{hydr} as compared to MgO(001),[56] as well as with the STM data presented in Figure 1.

The correlation of XPS and IRAS results discussed above allows for the following classification of Au species present at the initial stages of nucleation on hydroxylated MgO(001): The Au species on MgO_{hydr} with Au $4f_{7/2}$ binding energies in the range 86−87 eV, and CO stretching frequencies in the range 2165−2170 cm^{-1}, are assigned to small Au_xO_y aggregates. The second Au species exhibiting a binding energy of ~85 eV and a related CO IR signal at 2130 cm^{-1} correspond to small Au clusters with a few oxidized gold atoms at the oxide/cluster interface. The decrease of intensity of the XPS peak at 86−87 eV in the temperature range 100−300 K together with the increase of intensity of the lower binding energy component (Figure 5c) may be attributed either to decomposition of the small, strongly oxidized Au species or to agglomeration into larger but still partially oxidized Au particles.

To summarize, the results of this study provide clear evidence for the selective chemical interaction of Au atoms with hydroxyl groups on the MgO surface. Hydroxyl groups not only act as strong anchoring sites for Au atoms but also are able to oxidize gold, leading to small Au_xO_y aggregates with characteristic XPS and CO IRAS properties. Furthermore, the interaction of Au with only one type of hydroxyl groups highlights the site selectivity of this interaction and, in addition, provides information on the chemical properties of hydroxyl groups on MgO. The enhanced sinter stability of Au particles on MgO_{hydr} compared to MgO(001) reported previously may consequently be explained by the enhanced interaction of Au particles with the MgO surface due to the formation of strong Au−O interfacial bonds, which hampers diffusion and aggregation as the temperature is increased.

It is interesting to compare the present results with previous Au nucleation studies on differently functionalized TiO_2(110) surfaces performed in UHV. Matthey et al.[35] found that Au homogeneously nucleates on the terraces of reduced, r-TiO_2, and oxidized, o-TiO_2, surfaces, whereas agglomeration to larger particles and decoration of step edges was observed for a hydrated, h-TiO_2, sample. Although not obvious at first sight, these findings are in agreement with what is reported here. The h-TiO_2 surface is prepared by H_2O dissociation at O-vacancy defects, leading to the formation of bridging hydroxyl groups, OH_{br}. Therefore, h-TiO_2 can essentially be described as H adatoms capping some of the bridging oxygen of a stoichiometric TiO_2(110) surface. Corresponding DFT calculations revealed low diffusion barriers for Au on h-TiO_2, in agreement with the experimental finding.[35] The chemical properties of this type of OH_{br} are clearly different from the dicoordinated hydroxyl groups that are involved in oxidation of Au on MgO_{hydr}. Our results should, therefore, be compared with the behavior of Au on o-TiO_2. According to DFT, small gold clusters interacting with O adatoms on o-TiO_2 become cationic and exhibit large adhesion energies.[35] The same behavior is found in the present study for the interaction of Au with OH on MgO_{hydr}, which suggests that dicoordinated hydroxyl groups with a stretching frequency of ν(OD) = 2737 cm^{-1} [or ν(OH) = 3710 cm^{-1}] interact in a similar way with Au as O adatoms on TiO_2. This conclusion is also in agreement with the finding that treatment of TiO_2 powder with aqueous pH 10 solution enhances the sinter resistance of small Au particles on this surface as compared to untreated TiO_2, which has been related to the formation of strongly bound hydroxyl groups.[23]

The presence of hydroxyl groups on the supporting oxide is an important factor in determining the dispersion of gold particles during the frequently employed deposition−precipitation method for the preparation of supported gold catalysts.[21,22] The present study carried out on a model oxide surface fully supports this assumption. Although the nature of the precursor, Au−hydroxyl complex in deposition−precipitation, as opposed to Au atoms in the present study, is clearly different, we notice various similarities in the XPS and CO IRAS signatures in the present work on hydroxylated MgO and powder samples prepared by the deposition−precipitation method.[13,57] For example, after thermal treatment of a freshly prepared Au/Al_2O_3 sample at 473 K in vacuum, which leads to decomposition of the Au−hydroxide complex and the formation of oxidic gold, Hadjiivanov and co-workers[57] observed a CO IR signal at 2167 cm^{-1} and assigned this to CO adsorbed on Au^+. In addition, after oxidation of metallic Au clusters, an IR signal at 2139 cm^{-1} was observed due to partially oxidized gold particles. The CO stretching frequencies of the two Au species reported by Hadjiivanov and co-workers[57] agree well with those reported in the present study observed after Au deposition on hydroxylated MgO. We take this as clear evidence that the chemical identity of the gold species found on the hydroxylated MgO model system is the same as those that are frequently observed in real catalyst samples. Moreover, careful analysis of the data presented here allows for an unambiguous correlation of IR and XPS signals of these gold species.

Finally, we point out that the finding of enhanced stability of Au particles on a hydroxylated oxide surface, which holds for MgO(001) and TiO_2(110) with terminal OH(OD) groups, may not generally be applied to other metal/oxide systems. For example, the opposite trend, higher adhesion energies on non-hydroxylated surfaces, is predicted in calculations for Pd_{13} on γ-Al_2O_3, which is explained by the strong Pd−Al bond that forms on the nonhydroxylated surface and cannot be established on the hydroxylated one.[58]

5. CONCLUSION

This study presents a detailed experimental investigation of the reactivity of MgO-supported gold toward water vapor and surface hydroxyl groups. The interaction of small supported gold particles with water in the millibar pressure range leads to changes in the electronic structure due to partial oxidation of the particles with hydroxyl groups. Hydroxyl groups present on the MgO(001) surface prior to gold deposition have been shown to influence the nucleation, bonding, and electronic structure of gold on the MgO(001) surface in a wide temperature range.

The results presented here show that gold atoms are reactive toward oxidation when deposited onto hydroxylated MgO. The IR data provide clear evidence for a selective OH−Au interaction, which is found to affect only dicoordinated OH groups. The stronger interaction of Au with the hydroxylated MgO surface due to the formation of strong Au−O interfacial bonds is responsible for the enhanced thermal stability and, hence, the higher gold dispersion on hydroxylated as compared to clean MgO(001). Finally, the comparative infrared and photoemission results presented here are in good agreement with data from powder samples at the various stages of their preparation history and enable a direct correlation of the chemical nature of Au and the respective spectroscopic signatures.

■ ASSOCIATED CONTENT

Supporting Information. Additional text describing the XPS fitting procedure and one figure showing XPS spectra of Au 4f and Mg 2p regions for 0.02 ML Au on MgO(001), $MgO_{hydr(l)}$, and $MgO_{hydr(h)}$ at various annealing temperatures (100, 200, 300, and 573 K). This material is available free of charge via the Internet at http://pubs.acs.org.

■ AUTHOR INFORMATION

Corresponding Author
sterrer@fhi-berlin.mpg.de

■ ACKNOWLEDGMENT

The work has been supported by the Deutsche Forschungsgemeinschaft through the Cluster of Excellence "UNICAT" administered by the TU Berlin. M.A.B. and F.S. thank the Alexander-von-Humboldt Foundation for fellowships. Y.F. is grateful to Co. Ltd. Takata and DAAD for a fellowship.

■ REFERENCES

(1) Boehm, H.-P.; Knözinger, H. In *Catalysis: Science and Technology*; Anderson, J. R., Knözinger, H., Eds.; Springer: Berlin, 1983; Vol. 4, p 39.
(2) Averseng, F.; Vennat, M.; Che, M. In *Handbook of Heterogeneous Catalysis*; Ertl, G., Knözinger, H., Schüth, F., Weitkamp, J., Eds.; VCH: Weinheim, Germany, 2008; Vol. 2, p 522.
(3) Kung, M. C.; Davis, R. J.; Kung, H. H. *J. Phys. Chem. C* **2007**, *111*, 11767.
(4) Campbell, C. T. *Surf. Sci. Rep.* **1997**, *27*, 1.
(5) Freund, H.-J. *Angew. Chem., Int. Ed.* **1997**, *36*, 452.
(6) Henry, C. R. *Surf. Sci. Rep.* **1998**, *31*, 235.
(7) Fu, Q.; Wagner, T. *Surf. Sci. Rep.* **2007**, *62*, 431.
(8) Chambers, S. A.; Droubay, T.; Jennison, D. R.; Mattsson, T. R. *Science* **2002**, *297*, 827.
(9) Bond, G. C.; Louis, C.; Thompson, D. T. *Catalyis by Gold*; Catalytic Science Series; Hutchings, G. J., Ed.; Imperial College Press: London, 2006.
(10) Haruta, M.; Tsubota, S.; Kobayashi, T.; Kageyama, H.; Genet, M. J.; Delmon, B. *J. Catal.* **1993**, *144*, 175.
(11) Herzing, A. A.; Kiely, C. J.; Carley, A. F.; Landon, P.; Hutchings, G. J. *Science* **2008**, *231*, 1331.
(12) Lopez, N.; Janssens, T. V. W.; Clausen, B. S.; Xu, Y.; Mavrikakis, M.; Bligaard, T.; Norskov, J. K. *J. Catal.* **2004**, *223*, 232.
(13) Park, E. D.; Lee, I. S. *J. Catal.* **1999**, *186*, 1.
(14) Bond, G. C.; Thompson, G. T. *Gold Bull.* **2000**, *33*, 41.
(15) Guzman, J.; Gates, B. C. *J. Am. Chem. Soc.* **2004**, *126*, 2672.
(16) Widmann, D.; Liu, Y.; Schüth, F.; Behm, R. J. *J. Catal.* **2010**, *276*, 292.
(17) Jia, C.-J.; Liu, Y.; Bongard, H.; Schüth, F. *J. Am. Chem. Soc.* **2010**, *132*, 1520.
(18) Daté, M.; Okumura, M.; Tsubota, S.; Haruta, M. *Angew. Chem., Int. Ed.* **2004**, *43*, 2129.
(19) Gao, F.; Wood, T. E.; Goodman, D. W. *Catal. Lett.* **2010**, *134*, 9.
(20) Diemant, T.; Bansmann, J.; Behm, R. J. *Vacuum* **2010**, *84*, 193.
(21) Moreau, F.; Bond, G. C.; Taylor, A. O. *J. Catal.* **2005**, *231*, 105.
(22) Qian, K.; Fang, J.; Huang, W.; He, B.; Jiang, Z.; Ma, Y.; Wei, S. *J. Mol. Catal. A: Chem.* **2010**, *320*, 97.
(23) Veith, G. M.; Lupini, A. R.; Dudney, N. J. *J. Phys. Chem. C* **2009**, *113*, 269.
(24) Cunningham, D. A. H.; Vogel, W.; Haruta, M. *Catal. Lett.* **1999**, *63*, 43.
(25) Qiao, B.; Zhang, J.; Liu, L.; Deng, Y. *Appl. Catal., A* **2008**, *340*, 220.
(26) Libuda, J.; Frank, M.; Sandell, A.; Andersson, S.; Brühwiler, P. A.; Bäumer, M.; Mårtensson, N.; Freund, H.-J. *Surf. Sci.* **1997**, *384*, 106.
(27) Starr, D. E.; Diaz, S. F.; Musgrove, J. E.; Ranney, J. T.; Bald, D. J.; Nelen, L.; Ihm, H.; Campbell, C. T. *Surf. Sci.* **2002**, *515*, 13.
(28) Jensen, M. C. R.; Venkataramani, K.; Helveg, S.; Clausen, B. S.; Reichling, M.; Besenbacher, F.; Lauritsen, J. V. *J. Phys. Chem. C* **2008**, *112*, 16953.
(29) Fu, Q.; Wagner, T.; Rühle, M. *Surf. Sci.* **2006**, *600*, 4870.
(30) Niu, C.; Shepherd, K.; Martini, D.; Tong, J.; Kelber, J. A.; Jennison, D. R.; Bogicevic, A. *Surf. Sci.* **2000**, *465*, 163.
(31) Lazzari, R.; Jupille, J. *Phys. Rev. B* **2005**, *71*, No. 045409.
(32) Fajín, J. L. C.; Cordeiro, M. N. D. S.; Illas, F.; Gomes, J. R. B. *J. Catal.* **2010**, *276*, 92.
(33) Mavrikakis, M.; Stoltze, P.; Norskov, J. K. *Catal. Lett.* **2000**, *64*, 101.
(34) Wang, J. G.; Hammer, B. *Phys. Rev. Lett.* **2006**, *97*, No. 136107.
(35) Matthey, D.; Wang, J. G.; Wendt, S.; Matthiesen, J.; Schaub, R.; Laegsgaard, E.; Hammer, B.; Besenbacher, F. *Science* **2007**, *315*, 1692.
(36) Wu, T.; Kaden, W. E.; Anderson, S. L. *J. Phys. Chem. C* **2008**, *112*, 9006.
(37) Tong, X.; Benz, L.; Chrétien, S.; Metiu, H.; Bowers, M. T.; Buratto, S. K. *J. Phys. Chem. C* **2010**, *114*, 3987.
(38) Carrasco, E.; Brown, M. A.; Sterrer, M.; Freund, H.-J.; Kwapien, K.; Sierka, M.; Sauer, J. *J. Phys. Chem. C* **2010**, *114*, 18207.
(39) Barcaro, G.; Fortunelli, A. *New J. Phys.* **2007**, *9*, 22.
(40) Heemeier, M.; Frank, M.; Libuda, J.; Wolter, K.; Kuhlenbeck, H.; Bäumer, M.; Freund, H.-J. *Catal. Lett.* **2000**, *68*, 19.
(41) Giorgio, S.; Cabié, M.; Henry, C. R. *Gold Bull.* **2008**, *41*, 167.
(42) Mason, M. G. *Phys. Rev. B* **1983**, *27*, 748.
(43) Pireaux, J. J.; Liehr, M.; Thiry, P. A.; Delrue, J. P.; Caudano, R. *Surf. Sci.* **1984**, *141*, 221.
(44) Wertheim, G. K.; Di Cenzo, S. B.; Youngquist, S. E. *Phys. Rev. Lett.* **1983**, *51*, 2310.
(45) Lee, S.; Fan, C. Y.; Wu, T. P.; Anderson, S. L. *Surf. Sci.* **2005**, *578*, 5.
(46) Torelli, P.; Giordano, L.; Benedetti, S.; Luches, P.; Annese, E.; Valeri, S.; Pacchioni, G. *J. Phys. Chem. C* **2009**, *113*, 19957.
(47) Wagner, C. D.; Joshi, A. *J. Electron Spectrosc. Relat. Phenom.* **1988**, *47*, 283.
(48) Brown, M. A.; Ringleb, F.; Fujimori, Y.; Sterrer, M.; Freund, H.-J.; Preda, G.; Pacchioni, G. *J. Phys. Chem. C* **2011**, *115*, 10114.
(49) Chusuei, C. C.; Lai, X.; Luo, K.; Goodman, D. W. *Top. Catal.* **2001**, *14*, 71.
(50) Mihaylov, M.; Knözinger, H.; Hadjiivanov, K.; Gates, B. C. *Chem. Ing. Tech.* **2007**, *79*, 795.
(51) Knözinger, E.; Jakob, K.-H.; Singh, S.; Hofmann, P. *Surf. Sci.* **1993**, *290*, 388.
(52) Chizallet, C.; Costentin, G.; Che, M.; Delbecq, F.; Sautet, P. *J. Am. Chem. Soc.* **2007**, *129*, 6442.

(53) Finocchi, F.; Hacquart, R.; Naud, C.; Jupille, J. *J. Phys. Chem. C* **2008**, *112*, 13226.
(54) Savio, L.; Smerieri, M.; Orzelli, A.; Vattuone, L.; Rocca, M.; Finocchi, F.; Jupille, J. *Surf. Sci.* **2010**, *604*, 252.
(55) Ono, L. K.; Roldan Cuenya, B. *J. Phys. Chem. C* **2008**, *112*, 4676.
(56) Brown, M. A.; Carrasco, E.; Sterrer, M.; Freund, H.-J. *J. Am. Chem. Soc.* **2010**, *132*, 4064.
(57) Venkov, T.; Klimev, H.; Centeno, M. A.; Odriozola, J. A.; Hadjiivanov, K. *Catal. Commun.* **2006**, *7*, 308.
(58) Hu, C. H.; Chizallet, C.; Mager-Maury, C.; Corral-Valero, M.; Sautet, P.; Toulhoat, H.; Raybaud, P. *J. Catal.* **2010**, *274*, 99.